

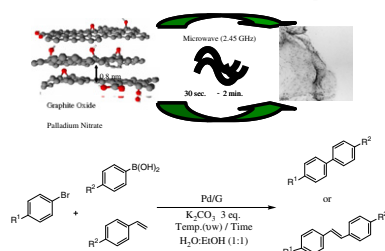


Contents

REGULAR ARTICLES

Microwave-assisted synthesis of palladium nanoparticles supported on graphene: A highly active and recyclable catalyst for carbon–carbon cross-coupling reactions pp 1–11

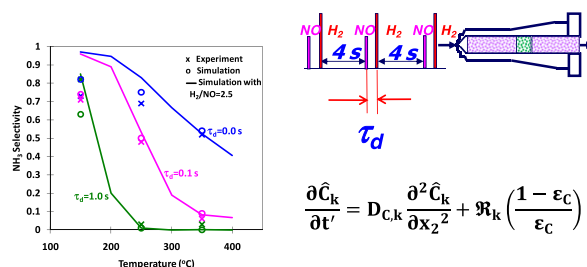
Ali R. Siamaki, Abd El Rahman S. Khder, Victor Abdelsayed, M. Samy El-Shall*, B. Frank Gupton*



Highly active and recyclable Pd/graphene catalyst for cross-coupling reactions.

Microkinetic modeling of the NO + H₂ system on Pt/Al₂O₃ catalyst using temporal analysis of products pp 12–26

Ashok Kumar, Xiaolin Zheng, Michael P. Harold*, Vemuri Balakotaiah*



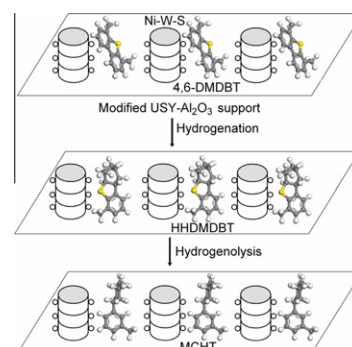
Temporal Analysis of Products (TAP) was used to probe the transient kinetics of the NO+H₂ on Pt reaction system. A microkinetic description of the catalytic chemistry was incorporated into a TAP model. The model predicted most of the main features of the data such as the variation in the NH₃ selectivity with the temperature for different delay times (τ_d) between the NO and H₂ pulses.

Citric acid-assisted hydrothermal method for preparing NiW/USY–Al₂O₃ ultradeep hydrodesulfurization catalysts

pp 27–35

Yu Fan, Han Xiao, Gang Shi, Haiyan Liu, Ying Qian, Tinghai Wang, Guangbi Gong, Xiaojun Bao*

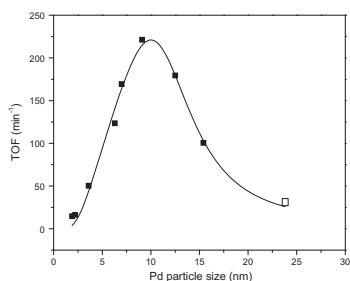
A novel method for coupling the citric acid-assisted hydrothermal dispersion of active metals and the hydrothermal modification of HY zeolite was proposed, which endows the resulting NiW/USY–Al₂O₃ catalyst with outstanding hydrogenation and hydrogenolysis activities for hydrodesulfurizing 4,6-DMDBT.



Structure sensitivity of dodecahydro-N-ethylcarbazole dehydrogenation over Pd catalysts

pp 36–47

Farnaz Sotoodeh, Kevin J. Smith*

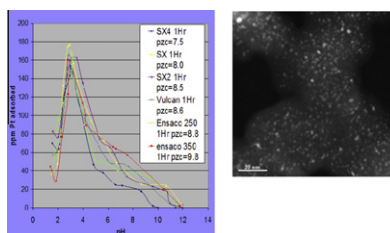


The complete recovery of the H₂ stored on dodecahydro-N-ethylcarbazole is reported at 443 K and 101 kPa using Pd/SiO₂ catalysts prepared by wet impregnation and calcination in He. The dehydrogenation TOF and selectivity to the completely dehydrogenated product, N-ethylcarbazole, were dependent upon Pd particle size. The structure sensitivity of the reaction and the observed product distribution are supported by results from DFT calculations.

A fundamental study of Pt impregnation of carbon: Adsorption equilibrium and particle synthesis

pp 48–65

X. Hao, S. Barnes, J.R. Regalbuto*

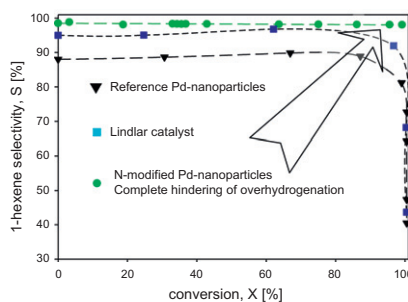


Carbons of like PZC exhibit a similar sharp optimum in adsorption pH, at which 1–2-nm particles can be synthesized at high Pt loading.

Supported nitrogen-modified Pd nanoparticles for the selective hydrogenation of 1-hexyne

pp 66–74

Micaela Crespo-Quesada, Ryan R. Dykeman, Gabor Laurenczy, Paul J. Dyson, Lioubov Kiwi-Minsker*

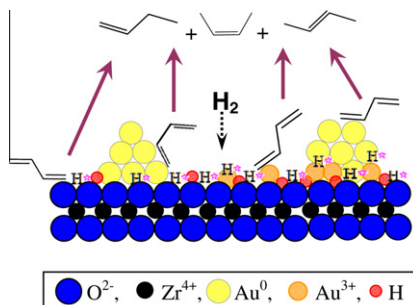


Supported N-modified Pd nanoparticles selectively catalyze 1-hexyne hydrogenation to 1-hexene, demonstrating a remarkable increase in the selectivity through a site-blocking effect and complete hindering of the over-hydrogenation to 1-hexane.

Vital roles of hydroxyl groups and gold oxidation states in Au/ZrO₂ catalysts for 1,3-butadiene hydrogenation

pp 75–87

Xin Zhang, Hui Shi, Bo-Qing Xu*



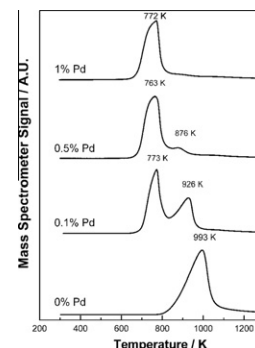
Active Au/ZrO₂ catalysts for 1,3-butadiene hydrogenation are composed of OH-carrying ZrO₂, metallic Au⁰ nanoparticles and/or Au³⁺ ions. In the absence of isolated surface Au³⁺ ions, the activation of H₂ in the reaction occurs on ensembles involving metallic Au⁰ atoms and OH-groups on ZrO₂ or containing Au⁰ atoms and Au³⁺ ions.

Lowering the synthesis temperature of Ni₂P/SiO₂ by palladium addition

V. Teixeira da Silva*, L.A. Sousa, R.M. Amorim, L. Andrini, S.J.A. Figueroa, F.G. Requejo, Flavio C. Vicentini

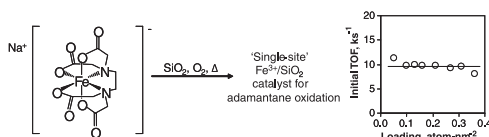
Addition of small amounts of palladium to a nickel phosphate supported on silica sample lead to a decrease of ~200 K in the synthesis temperature of Ni₂P/SiO₂.

pp 88–102

**Surface speciation and alkane oxidation with highly dispersed Fe(III) sites on silica**

Dario Prieto-Centurion, Justin M. Notestein*

pp 103–110

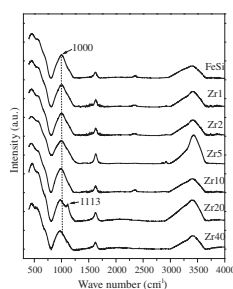


Impregnation of SiO₂ with aqueous NaFeEDTA, followed by oxidative heat treatment to 800 °C, produces highly dispersed Fe³⁺ species. For adamantane oxidation by H₂O₂ to alcohols and ketones, these materials show constant initial TOF with Fe loading – indicating 'single-site' catalysts.

Modification of Fe–SiO₂ interaction with zirconia for iron-based Fischer–Tropsch catalysts

Ming Qing, Yong Yang*, Baoshan Wu, Jian Xu, Chenghua Zhang, Peng Gao, Yongwang Li

pp 111–122

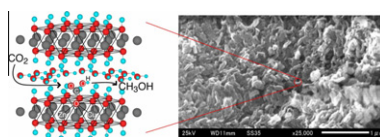


FTIR results show that Fe–SiO₂ interaction could be well explained in terms of the formation of Fe–O–Si bond, and this interaction can be weakened by ZrO₂.

Photocatalytic conversion of carbon dioxide into methanol using zinc–copper–M(III) (M = aluminum, gallium) layered double hydroxides

Naveed Ahmed, Yoshiyuki Shibata, Tatsuo Taniguchi, Yasuo Izumi*

pp 123–135

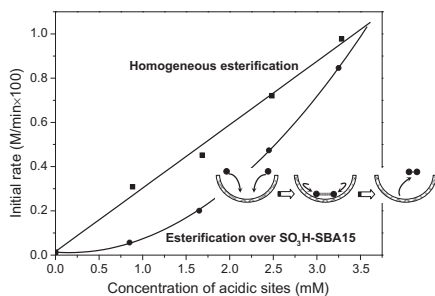


Under the UV–visible light in CO₂ + H₂, Zn–Al layered double hydroxide was most active to mainly form CO and Zn–Cu–Ga LDH was most selective to produce methanol (68 mol%).

Mechanism of acetic acid esterification over sulfonic acid-functionalized mesoporous silica

pp 136–143

Shaojun Miao, Brent H. Shanks*

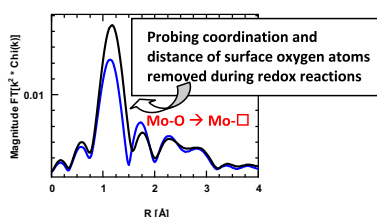


Esterification was found to occur via a dual site mechanism over a propylsulfonic acid-functionalized mesoporous silica catalyst in contrast to the Eley-Rideal mechanism with the homogeneous propane sulfonic acid.

Mechanistic insights into the formation of acetaldehyde and diethyl ether from ethanol over supported VO_x, MoO_x, and WO_x catalysts

pp 144–154

Hari Nair, Joseph E. Gatt, Jeffrey T. Miller, Chelsey D. Baertsch*

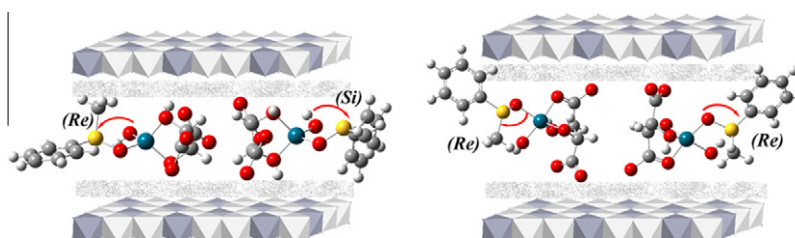


Mechanisms for ethanol oxidative dehydrogenation to acetaldehyde and condensation to diethyl ether over supported metal oxides of molybdenum, tungsten and vanadium have been proposed. Through the use of spectroscopy and kinetic studies, it is shown that the oxygen linking the active metal atom to the support is the active oxygen for acetaldehyde formation.

Orientated intercalation of tartrate as chiral ligand to impact asymmetric catalysis

pp 155–162

Huimin Shi, Jing He*



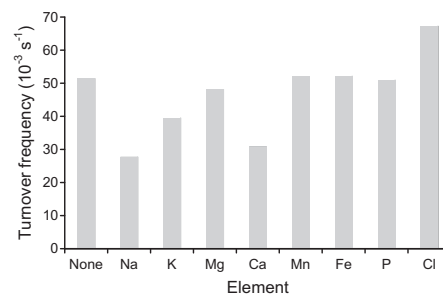
The tartrate orientation in the interlayer region of LDHs influences the coordination modes of tartrate as ligand to Ti (IV) centers and the asymmetric catalysis in the heterogeneous sulfoxidation of pro-chiral methyl phenyl sulfide.

Effect of biomass-derived synthesis gas impurity elements on cobalt Fischer–Tropsch catalyst performance including *in situ* sulphur and nitrogen addition

pp 163–173

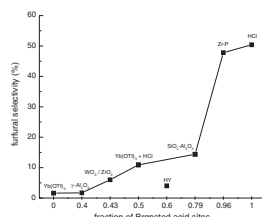
Øyvind Borg, Nina Hammer, Bjørn Christian Enger, Rune Myrstad, Odd Asbjørn Lindvåg, Sigrd Eri, Torild Hulsund Skagseth, Erling Rytter*

The effect of typical biomass-derived synthesis gas impurities on the cobalt Fischer–Tropsch (FT) performance was investigated at industrially relevant conditions. Significant variations in turnover frequency and product selectivity were observed.



Design of solid acid catalysts for aqueous-phase dehydration of carbohydrates: The role of Lewis and Brønsted acid sites pp 174–182

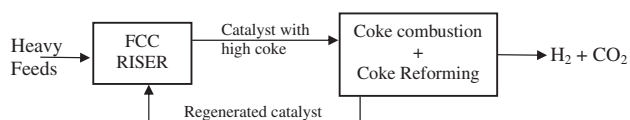
Ronen Weingarten, Geoffrey A. Tompsett, Wm Curtis Conner Jr., George W. Huber*



Furfural selectivity increases with an increase in the Brønsted to Lewis acid site ratio of the catalyst. Lewis acid sites decrease furfural selectivity by catalyzing a side reaction between xylose and furfural to form humins. A low furfural selectivity was observed with HY zeolite due to strong irreversible adsorption of the furfural in the micropores, causing an increase in the rate of humin formation.

Coke steam reforming in FCC regenerator: A new mastery over high coking feeds pp 183–195

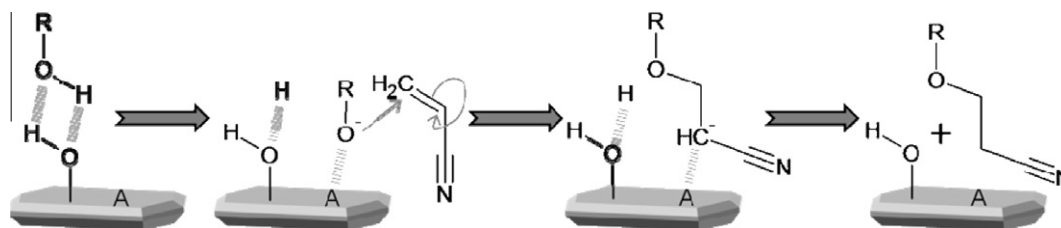
Avelino Corma*, Laurent Sauvanaud, Eric Dorskocil, George Yaluris



FCC catalysts with high coke-on-catalyst can be regenerated without temperature constraints by combining coke combustion (exothermic) and coke reforming (endothermic), while producing hydrogen.

Cyanoethylation of alcohols by activated Mg–Al layered double hydroxides: Influence of rehydration conditions and Mg/Al molar ratio on Brønsted basicity pp 196–204

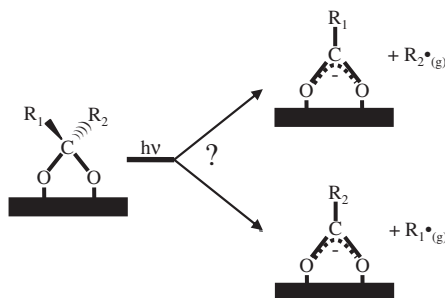
Jaime S. Valente*, Heriberto Pfeiffer, Enrique Lima, Julia Prince, Jorge Flores



Proposed mechanism by which activated MgAl LDHs catalyze the cyanoethylation of alcohols.

Generation of organic radicals during photocatalytic reactions on TiO₂ pp 205–212

M.A. Henderson*, N.A. Deskins, R.T. Zehr, M. Dupuis

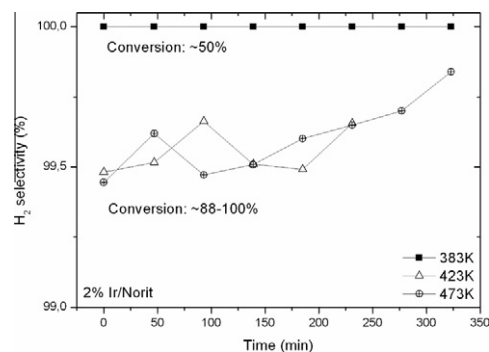


Ejection of organic radicals from TiO₂ surfaces during photocatalysis under applied conditions is prevalent based on model studies. In the case of organic carbonyl photodecomposition on TiO₂, preferred pathways for ejection of gas-phase organic radicals are predicted using DFT calculations and demonstrated using photodesorption.

Production of CO-free H₂ from formic acid. A comparative study of the catalytic behavior of Pt metals on a carbon support

pp 213–219

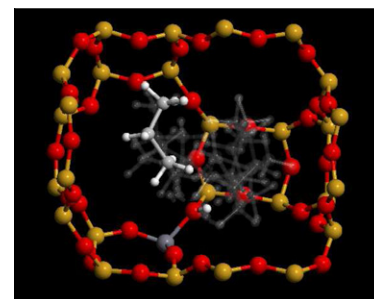
F. Solymosi*, Á. Koós, N. Liliom, I. Ugrai

CO-free H₂ was produced via steam reforming of formic acid on Ir catalyst deposited on carbon Norit.**Monomolecular cracking of propane over acidic chabazite: An ab initio molecular dynamics and transition path sampling study**

pp 220–228

Tomáš Bučko*, Lubomir Benco, Jürgen Hafner, János G. Ángyán

The monomolecular Haag-Dessau mechanism for propane cracking over acidic chabazite has been studied using dispersion-corrected periodic DFT calculations in combination with ab-initio molecular dynamics simulations, transition path sampling and free-energy gradient integrations. The preferred reaction mechanism and the intrinsic reaction parameters for the rate determining step have been determined.

**LETTERS TO THE EDITOR****Comments on “Shape-selective diisopropylation of naphthalene in H-mordenite: Myth or reality?”**

pp 229–230

Gyula Tasi, István Pálinkó*

Reply to the “Comments on Shape-selective diisopropylation of naphthalene in H-mordenite: Myth or reality?” by Gyula Tasi and István Pálinkó

p 231

Wim Buijs, Pierre A. Jacobs, Johan A. Martens*